Influence of resistivity on current and potential distribution of cathodic protection systems for steel framed masonry structures

LAMBERT, P. <http://orcid.org/0000-0002-2815-1674>, MANGAT, P. S. <http://orcid.org/0000-0003-1736-8891>, O'FLAHERTY, Fin <http://orcid.org/0000-0003-3121-0492> and WU, Y. Y.

Citation:

The Influence of Resistivity on the Current and Potential Distribution of Cathodic Protection Systems for Steel Framed Masonry Structures

P Lambert, P S Mangat & F J O'Flaherty

Centre for Infrastructure Management, Sheffield Hallam University, Howard Street, Sheffield, S1 1WB, United Kingdom

Y-Y Wu

CAPCIS, CAPCIS House, 1 Echo Street, Manchester, M1 7DP, United Kingdom

Abstract

This paper presents the influence of resistivity on the current and potential distribution of cathodic protection systems for steel framed masonry structures. The work involves both experimental measurements and boundary element analysis and follows on from earlier experiments employing sand as a simple model for masonry encasement that has been reported elsewhere. Factors such as the size and type of masonry, moisture content and width of mortar joints will affect the resistance of the path through which the cathodic protection currents pass and thereby influence the distribution onto the steel surface. To represent such variations in resistance it has been necessary to construct a small scale specimen replicating, as far as possible, actual applications on steel-framed structures. The results from the laboratory specimen and numerical modelling are in sufficient agreement to confirm the validity of the modelling approach and allow the results to be employed for design and development purposes.

Keywords: corrosion, masonry, steel frame, cathodic protection, impressed current, numerical modelling.

Introduction

Experimental and numerical studies on cathodic protection (CP) systems for steel framed masonry structures were conducted in previous work[1] employing moist sand as a model for masonry. This initial study assisted in the understanding of the distribution of potential and current to the surface of typical structural steel sections and the various influences on the distribution.

It was found that there could be a significant variation of protection potential and current density across the surface of the steel. This variation is related to the resistivity of electrolyte, the anode locations and the geometry of the steel section. The distribution of the CP potential and current density was confirmed to be directly related to the resistivity of electrolyte. Under the same applied current density and anode location, the distribution of the protection potential and current density was shown to be more uniform in a low resistivity electrolyte while a higher resistivity electrolyte resulted, as would be expected, in a lower protective current density on the surface of steel.

The anode position has a significant effect on the distribution of CP potential and current density. The potential and current density distributions along the surface of steel section become more uniform as the anode distance from the steel increases, an effect that is recognised in conventional CP of buried and submerged structures where the anodes can be located a considerable distance from the item to be protected.

A final conclusion from this initial study was that boundary element modelling[2] shows significant promise as a practical tool for analysing and optimising the design of cathodic protection system for steel framed masonry structures.

While damp sand is a convenient model for masonry and allows a range of steel and anode geometries to be study with relative ease, it does not accurately represent a typical masonry structure consisting of blocks of stone or fired clay with mortar jointing. The resistivities of most masonry materials are much higher than the mortars employed in steel-framed masonry structures. The specific resistivities of the various masonry materials such as brick and Portland stone are also different. As a result, any area of low resistivity may be expected to "attract" a higher current density, with current flowing preferentially along the path of least resistance[3].

This paper presents a study into the influence of resistivity on the current and potential distribution of cathodic protection system for steel framed masonry structures. This in turn relates to factors such as the type of masonry, size of masonry unit and the thickness of mortar beds and how they may influence the effectiveness of cathodic protection systems. The study employs many of the techniques developed for the sand study and incorporates both experimental measurements and boundary element analysis. The principles and basic components of impressed current cathodic protection (ICCP) systems as employed for the preservation of steel framed heritage structures are well documented and have been described elsewhere[4].

Experimental Procedure

A representative ICCP system was constructed to investigate the effect of the resistivity of brick masonry and joints width on CP current and potential. The basic components of this system were a DC power supply unit, comprising a commercial CP power supply system manufactured by Cathodic Protection International Aps; two Ebonex titanium oxide discrete anodes, 10mm diameter and 100mm in length, manufactured by Fosroc; a carbon steel ' I ' section as the cathode with dimensions as shown in Figure 1; a cement-lime mortar with mix proportions (by weight) of 1 cement : 2 lime : 9 sand, and a water-cement ratio of 0.5; and masonry in the form of fired clay 'common' brick with nominal dimensions of 215mm length, 102.5 mm width and 65mm height.

A test specimen of brickwork and mortar was constructed with the following dimensions; 440mm wide by 481mm long and 450mm high. Two discrete anodes, each 10mm diameter x 100mm length, were independently controlled to provide the protection current. They were located between the 3rd and 4th courses of bricks. The completed CP system is shown in Figures 2 and 3. A commercial embeddable silver/silver chloride/ 1M potassium chloride reference electrode was installed in the test specimen to evaluate levels of cathodic protection applied. The distance between the electrode axis and the steel surface was 5mm. After construction, the specimen was maintained at a constant 20°C and relative humidity of 60% for two weeks to allow substantial curing of the mortar.

The potential distribution on a grid of the exposed surfaces of the test specimen was measured under a range of test conditions, including variations in brick and masonry resistivity and output current, by means of a hand-held copper/copper sulphate electrode (CSE). However, potential values obtained in this manner do not represent the actual potentials on the surface of steel section due to the IR drop. In order to obtain values of the true CP protection potential on the surface of steel section, the instant-off potential method was employed. Due to the relatively complex geometry of the steel section it was not possible to accurately measure every point potential on the steel surface and therefore only the protection potentials were measured.

Boundary Element Method for Multi-Regional Problems

The boundary element method for single regions has been well described[2, 5]. In cases with two or more electrolyte materials in the region under study or when the component being analyzed is long and narrow, the model may be divided into a series of sub-regions or zones and the boundary element procedure applied to each sub-region in turn as if they were independent of each other. The final set of equations for the whole region can then be obtained by assembling the set of equations for each sub-region using the compatibility of potentials and current density between the common interfaces. Consider a two zone model as shown in Figure 4, with one zone called Ω^1 and the other Ω^2. The corresponding equations can be written as:

$$\begin{bmatrix} H^1 & H^1_I \end{bmatrix} \begin{Bmatrix} E^1 \\ E^1_I \end{Bmatrix} = \begin{bmatrix} G^1 & G^1_I \end{bmatrix} \begin{Bmatrix} i^1 \\ i^1_I \end{Bmatrix} \tag{1}$$

where E^1 and i^1 are the nodal potential and normal current density at the external boundary Γ^1, and E^1_I and i^1_I are the nodal potential and normal current density at the interface Γ_I.

Similarly, the matrix equation for the zone Ω^2 may be written as:

$$\begin{bmatrix} H^2 & H^2_I \end{bmatrix} \begin{Bmatrix} E^2 \\ E^2_I \end{Bmatrix} = \begin{bmatrix} G^2 & G^2_I \end{bmatrix} \begin{Bmatrix} i^2 \\ i^2_I \end{Bmatrix} \tag{2}$$

where E^2, i^2 are the nodal potential and normal current density at the external boundary Γ^2 respectively, E^2_I, i^2_I are the nodal potential and normal current density at the interface Γ_I.

The compatibility and equilibrium conditions on the interface Γ_I can be expressed as:

$$E^1_I = E^2_I = E_I \tag{3}$$

and:

$$i^1_I = -i^2_I = i_I \tag{4}$$

where E_I, i_I are potential and normal current density on the interface.

Using the above conditions in equations (3) and (4), the combined boundary element matrix equation can be written as:

$$\begin{bmatrix} H^1 & H_I^1 & \mathbf{O} \\ 0 & H_I^2 & \mathbf{H}^2 \end{bmatrix} \begin{Bmatrix} E^1 \\ E_I \\ E^2 \end{Bmatrix} = \begin{bmatrix} G^1 & G_I^1 & \mathbf{O} \\ 0 & -G_I^2 & \mathbf{G}^2 \end{bmatrix} \begin{Bmatrix} i^1 \\ i_I \\ i^2 \end{Bmatrix} \qquad (5)$$

As E_I and i_I are unknown at the interface the above system is also written as:

$$\begin{bmatrix} H^1 & H_I^1 & -G_I^1 & 0 \\ 0 & H_I^2 & G_I^2 & \mathbf{H}^2 \end{bmatrix} \begin{Bmatrix} E^1 \\ E_I \\ i_I \\ E^2 \end{Bmatrix} = \begin{bmatrix} G^1 & 0 \\ 0 & G^2 \end{bmatrix} \begin{Bmatrix} i^1 \\ i^2 \end{Bmatrix} \qquad (6)$$

This gives a matrix equation which is very similar to the original single zone equation[2, 5]. By applying the relevant boundary conditions, the equation can be solved.

The above method is important for accurately analysing cathodically protected steel-framed structures due to the different types of electrolyte such as brickwork, natural stone, faience (glazed terracotta), mortar and concrete that may be encountered. Furthermore, even for the same type of material the resistivity or conductivity will vary due to its composition, moisture content or location. For example, brick on the interior and exterior of a wall may have different moisture contents which could greatly influence the resistivity.

Results and Discussion

Electrical measurement obtained from the mortar demonstrated that it had a significantly lower resistivity than the surrounding brick. It was also noted that the resistivities of the mortar and bricks were consistent across the sepcimen. It is therefore considered that the whole of the mortar bed can reasonably be modelled as a single zone. Each brick has also been modelled as a separate zone. As the specimen was symmetrical in the X=0 and Y=0 directions, only half the model needed to be analyzed thereby simplifying the computation. The system was first analyzed under the following two cases which are symmetrical in the X=0 direction:

Case 1:

Average resistivity of mortar:	9.00 kΩ.cm.
Average resistivity of brick:	95.00 kΩ.cm.
Anode axis locations (X, Y, Z) cm:	Right (X=-5, Y=18.925, Z=23)
	Left (X=5, Y=18.925, Z=23).
Applied current density on the anodes:	4.20×10^{-2} mA/cm^2.

On completion, the anode was moved to the following location which was symmetrical in the Y=0 direction.

Case 2:

Average resistivity of mortar:	9.00 kΩ.cm.
Average resistivity of brick:	95.00 kΩ.cm.
Anode axis locations (X, Y, Z) cm:	Right (X =16.875, Y=-5, Z=23).
	Left (X=16.875, Y=5, Z=23).
Applied current density on the anodes:	4.20×10^{-2} mA/cm^2.

For both cases the boundary condition on the surface of the cathode (steel section) was based on experimentally measured polarization curves.

For Case 1, the total boundary element mesh used for the analysis is shown in Figure 5. The boundary element mesh on the steel surface is shown in Figure 6. Typical examples of the modelling results are shown in Figures 7 to 9. The total boundary element mesh used for the analysis of Case 2 is shown in Figure 10. The boundary element mesh on the steel surface is shown in Figure 11 and typical examples of the modelling results are given in Figures 12 and 13.

Cases 1 and 2 (Figure 9) show that there is a significant range in the potential distribution between the maximum and minimum values on the steel surface which is up to 48.75 % and 40.2% for Cases 1 and 2 respectively. Similarly, the change of current density distribution is also large. The range of the difference between maximum and minimum values is 88.58 % (Case 1) and 87.31% (Case 2). Therefore, it is apparent that for this arrangement the distribution of potential and current density on the surface of steel is noticeably non-uniform.

Cases 1 and 2 also illustrate the potential distribution in the electrolyte (brick and mortar). It has been demonstrated that the potential distribution in the electrolyte is not continuous. This may be due to differences in resistivity between the brick and mortar having an effect on the distribution of potential and current density throughout the electrolyte although there is no apparent periodic effect that can be associated with the resistivities and relative areas of the two materials.

Comparing the modelling results of the two cases, it is apparent that for each anode location the potential and current distribution on both the steel surface and in the electrolyte are completely different under the same modelling conditions. This demonstrates the key role played by the anode locations in the optimal distribution of the protective current in a CP system of this type.

In order to better understand the effect of the resistivity of brick and mortar on the distribution of potential and current density, the following additional cases (Cases 3 and 4) were analyzed. Consider the situation where the bricks in Cases 1 and 2 are removed and the steel is encased completely by mortar while the other modelling conditions remain the same. For ease of illustration, the details are shown below:

Case 3:

Average resistivity of mortar:	9.00 kΩ.cm.
Anode axis locations (X, Y, Z) cm:	Right (X=-5, Y=18.925, Z=23).
	Left (X=5, Y=18.925, Z=23).
Applied current density on the anodes:	4.20×10^{-2} mA/cm^2.

Case 4:

Average resistivity of mortar:	9.00 kΩ.cm.
Anode axis locations (X, Y, Z) cm:	Right (X=16.875, Y=-5, Z=23).
	Left (X=16.875, Y=5, Z=23).
Applied current density on the anodes:	4.20×10^{-2} mA/cm^2.

In each case the boundary condition on the surface of the cathode (steel section) was based on an experimentally measured polarization curve.

Under these conditions the two specimens can be considered to be homogeneous. They have been analyzed by the boundary element method for a single region. The total boundary element mesh used for the analysis of Case 3 is shown in Figure 14.

Comparing Case 1 with Case 3 demonstrates that the potential and current distributions on the steel surface in Case 3 are more uniform than in Case 1. Figure 9 shows that for Case 1 the maximum difference of potential distribution on the steel surface is 48.75 % while this value in Case 3 is 32.23%. The maximum difference in current distribution on the steel surface for Case 1 is 88.58 % while the corresponding value for Case 3 is 77.73%.

The above trend is also apparent when comparing Cases 2 and 4. In Case 2 the maximum difference of potential distribution on the steel surface is 40.20 % while this value for Case 4 is 29.19%. Figure 13 shows the difference of current distribution for Case 2 is 87.31% while the corresponding value in Case 4 is 72.52 %. Therefore, it is apparent that the potential and current distribution on the steel surface is more uniform when the steel is encased only in mortar.

Comparing the results from Cases 1 and 3 shows that the potential distribution in Case 3 is continuous whereas in Case 1 it is discontinuous. It can also be seen that the potential distribution in the electrolyte in Case 4 is continuous but in Case 2 it is discontinuous. These observations verify that the difference in resistivity between brick and mortar, brick type and the width of joints has a significant effect on the distribution of the potential and current density on the steel surface under the conditions of a fixed anode location and a given anode current.

The results of the boundary element modelling can now be compared with the experimental measurements. For simplicity, only the values of typical representative points have been selected for discussion. The results for both the boundary element solutions and the experimental data in Case 1, as shown in Figure 15, generally follow the same trend with a variation of no more than 15 % in the individual potential values. The cause for this difference could be associated with the experimental procedure, the method of modelling or both. For example, inaccurate experimental measurements could result from resistance drops in the cables and equipment or errors in data capture. In boundary element modelling, possible causes of inaccuracy could include errors in the experimentally obtained polarization curves or inaccurate discretisation of the element mesh. Although there is some difference

7

between the boundary element results and experimental data, the general level of agreement is sufficiently good to confirm the validity of the modelling approach and to allow the results to be employed for design purposes.

Conclusions

The work presented in this study leads to the following conclusions.

1. The difference in electrical resistivity between typical mortar and brick in masonry construction can be large. It has an effect on the distribution of the potential and current measured on the steel surface. Low resistivity mortar "attracts" a higher current density, with current flowing preferentially along the path of least electrical resistance. As a result, the distribution of potential and current on the steel surface is not uniform for any given anode location and anode current.

2. Boundary element modelling provides a powerful technique for analysing and optimising the design of cathodic protection system for steel framed masonry structures.

3. By employing the boundary element technique, it is possible to establish the influence of the masonry and mortar elements of construction. In this way the effect of masonry type, moisture condition and joint width can be factored into the design to ensure adequate and even protection of the steel by the cathodic protection system.

It is hoped that the output from this work can contribute the development of formal guidelines and standards for the cathodic protection of steel-framed masonry buildings.

Acknowledgements

References

1. Lambert, P., Mangat, P.S., O'Flaherty, F. J. & Wu, Y-Y. 'Experimental and Numerical Studies on the Cathodic Protection of Steel Framed Masonry Structures' *(In Press: Materials & Structures, RILEM, 2007).*
2. Brebbia, C.A., *The Boundary Element Method for Engineers,* Pentech Press, London, 1978.
3. Roberge, P.R., *Handbook of Corrosion Engineering*, McGraw-Hill,1999.
4. Lambert, P. & Wu, Y-Y, 'Electrochemical methods for the preservation of masonry clad structural frames, Maritime Heritage and Modern Ports', Proceedings of the Second International Conference on Maritime Heritage, Barcelona, 2005, pp 219-228.
5. Brebbia, C.A. & Dominguez, J., *The Boundary Elements - An Introductory Course,* McGraw-Hill, New York, 1989.
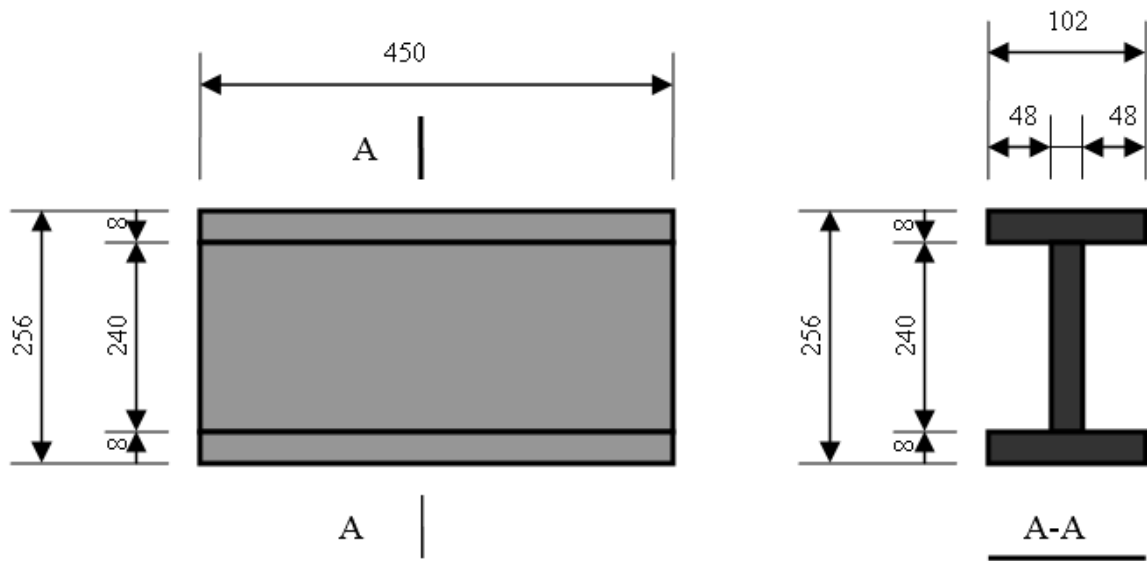
List of Figures
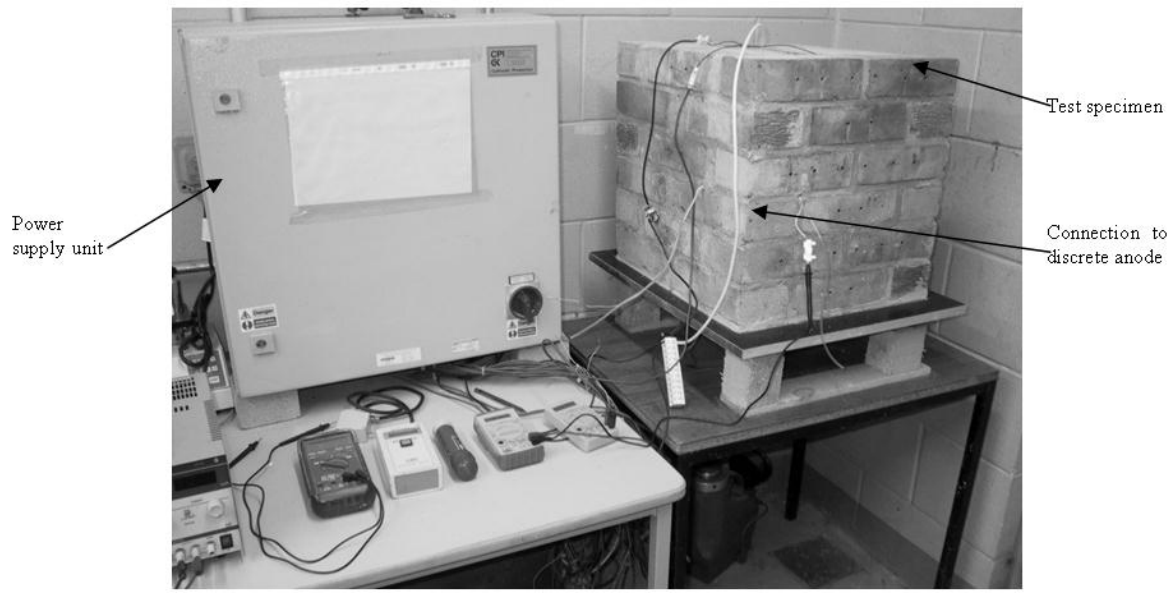
Figure 1: Steel section (unit: mm)
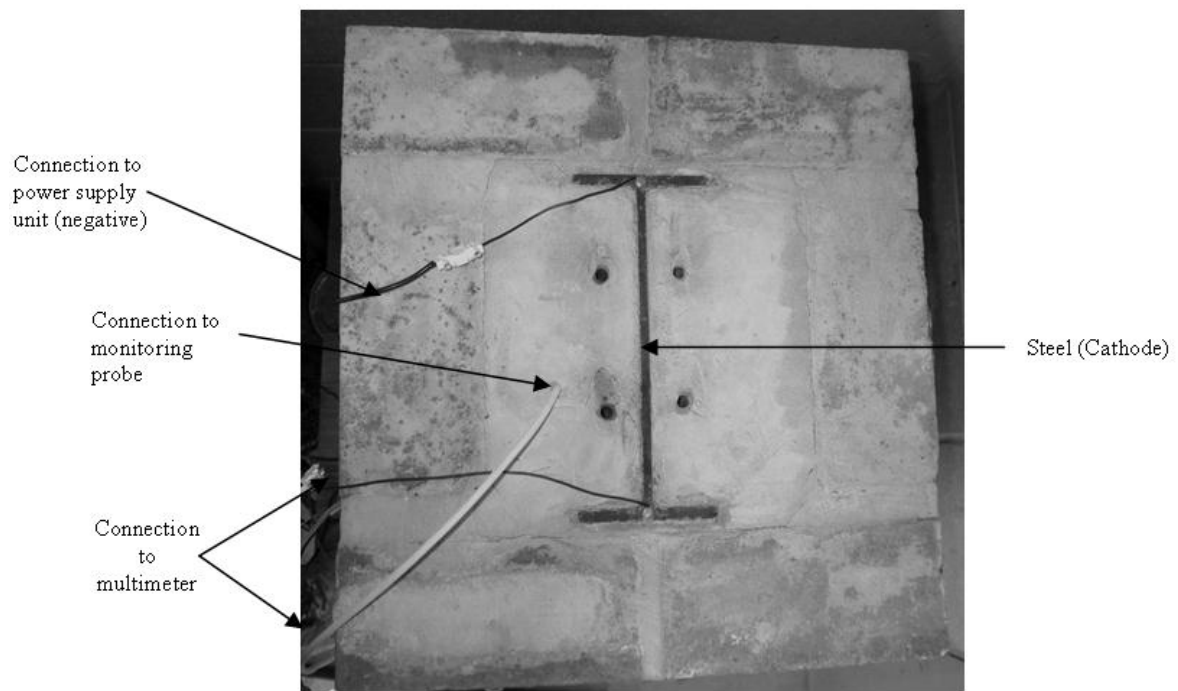
Figure 2: Experimental ICCP system

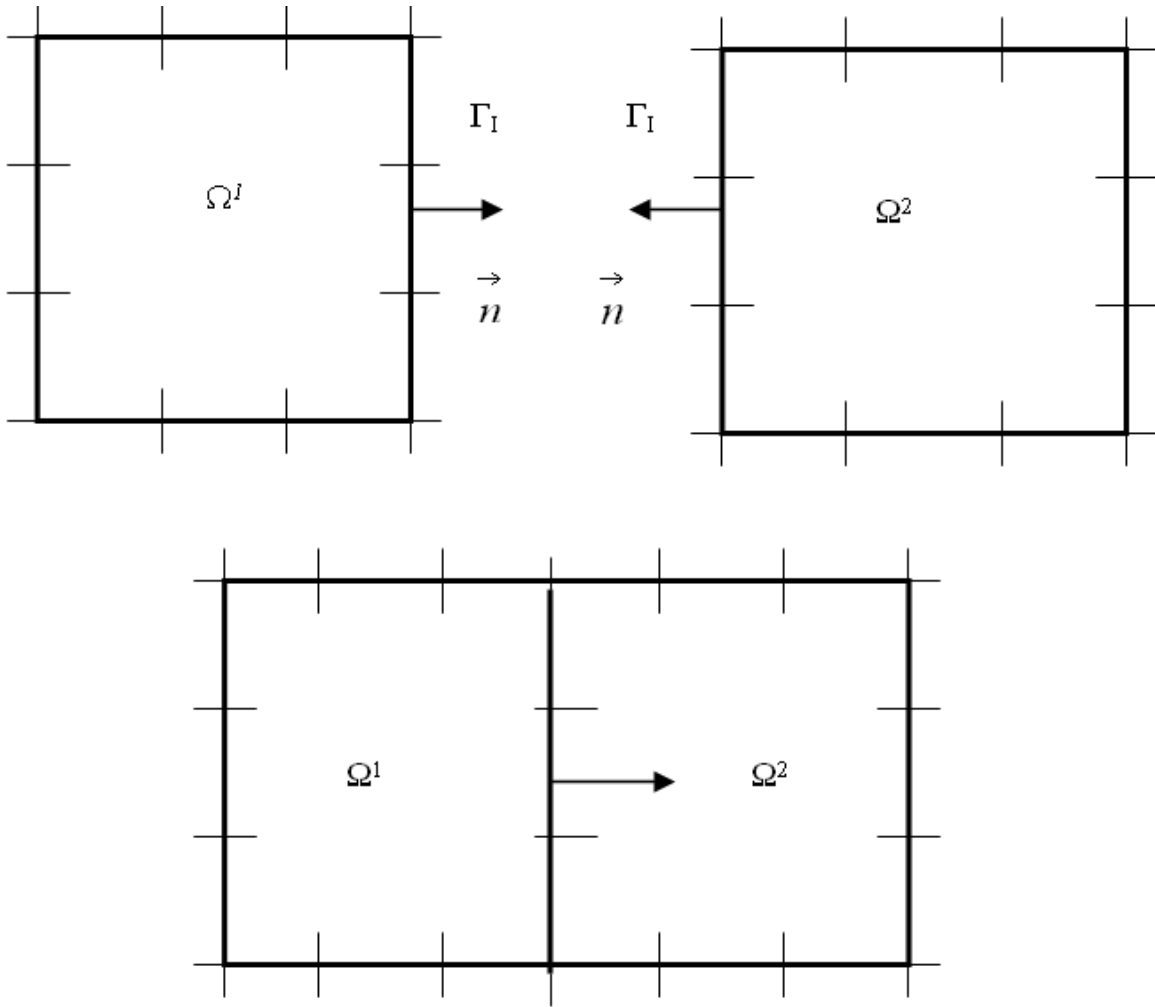Figure 3: Test specimen - plan view of ICCP system
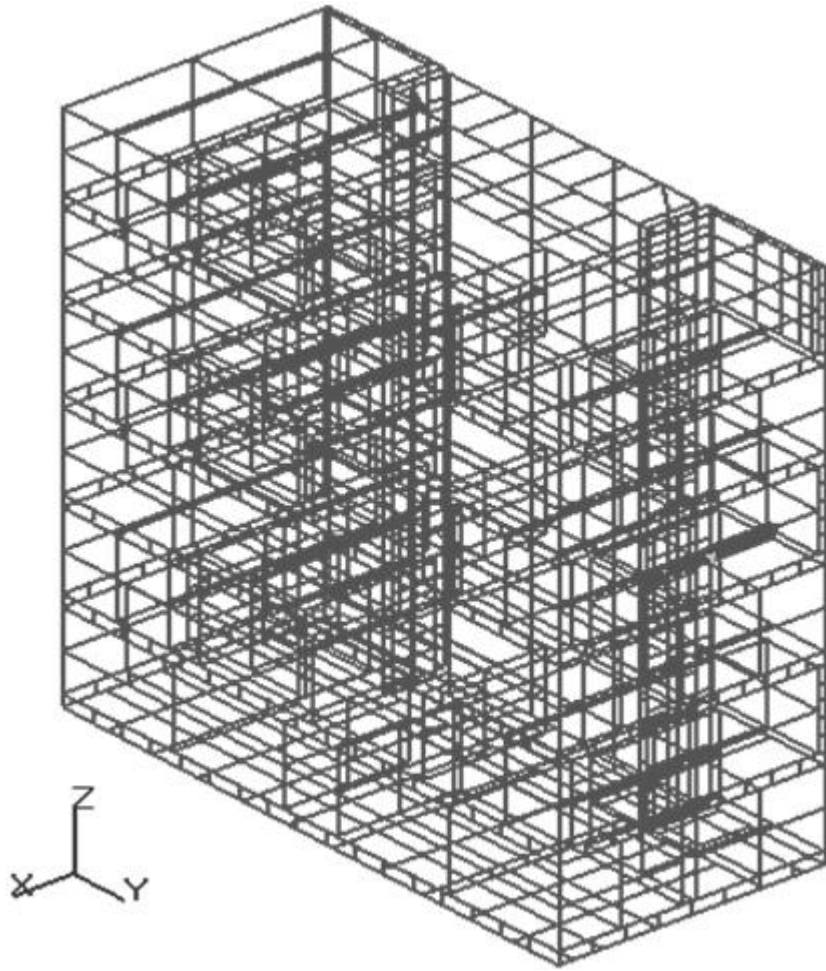
Figure 4: A model consisting of two zones

Figure 5: Schematic representation of the total boundary element mesh on the surface of the encased specimen (Case 1, symmetric in plane X=0)
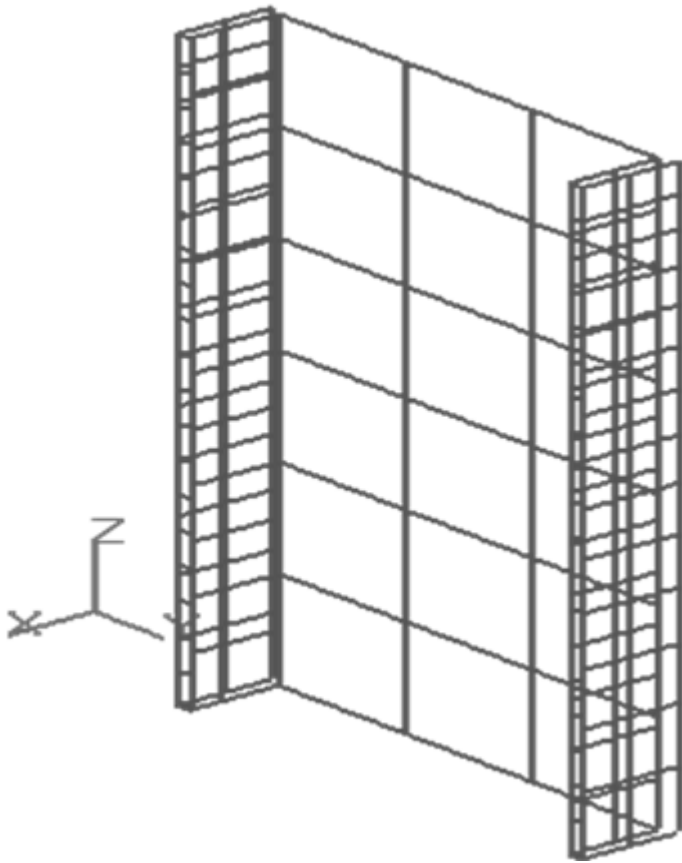
Figure 6: Schematic representation of the boundary element mesh on the surface of steel section (Case 1, symmetric in plane X=0)
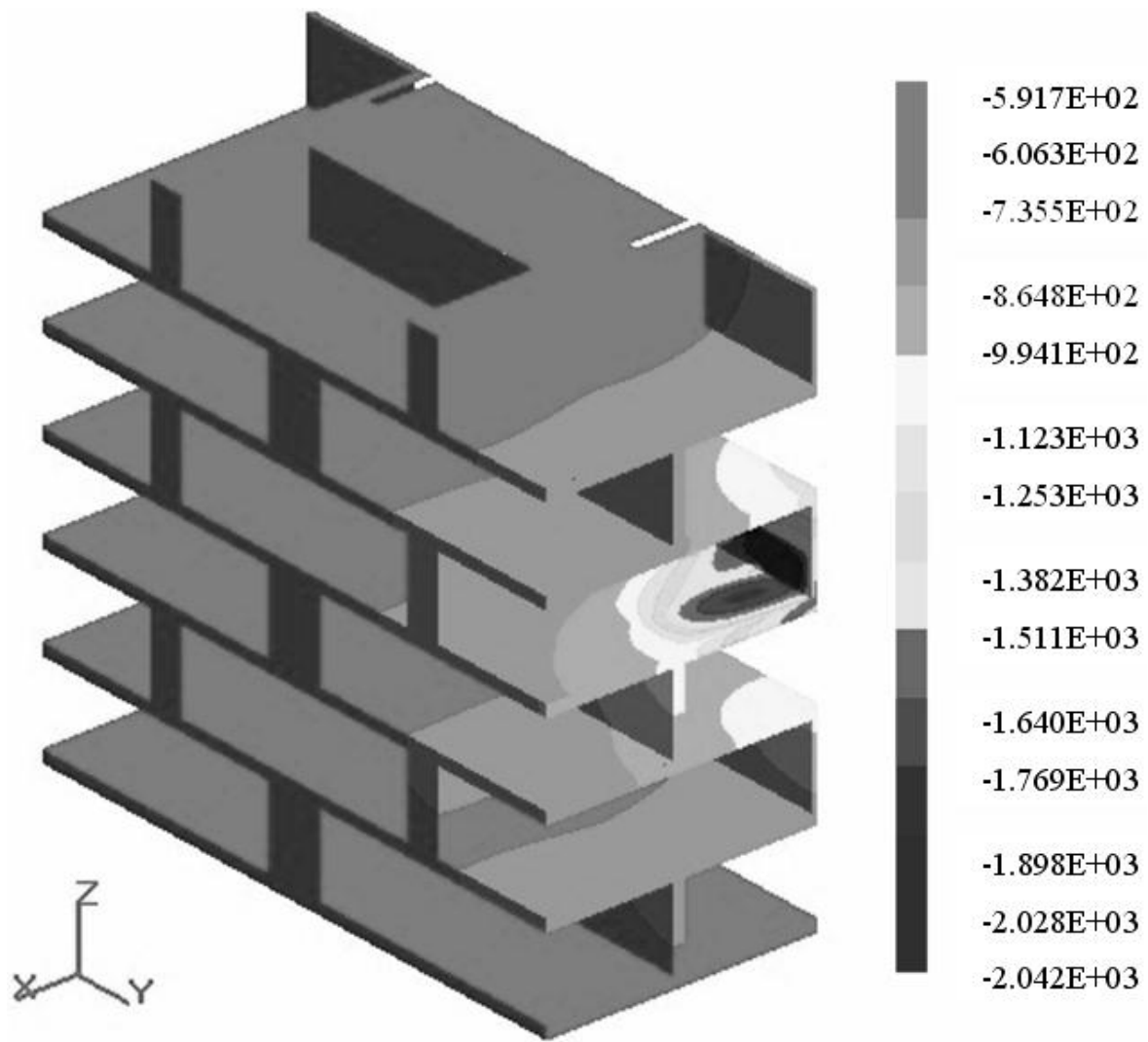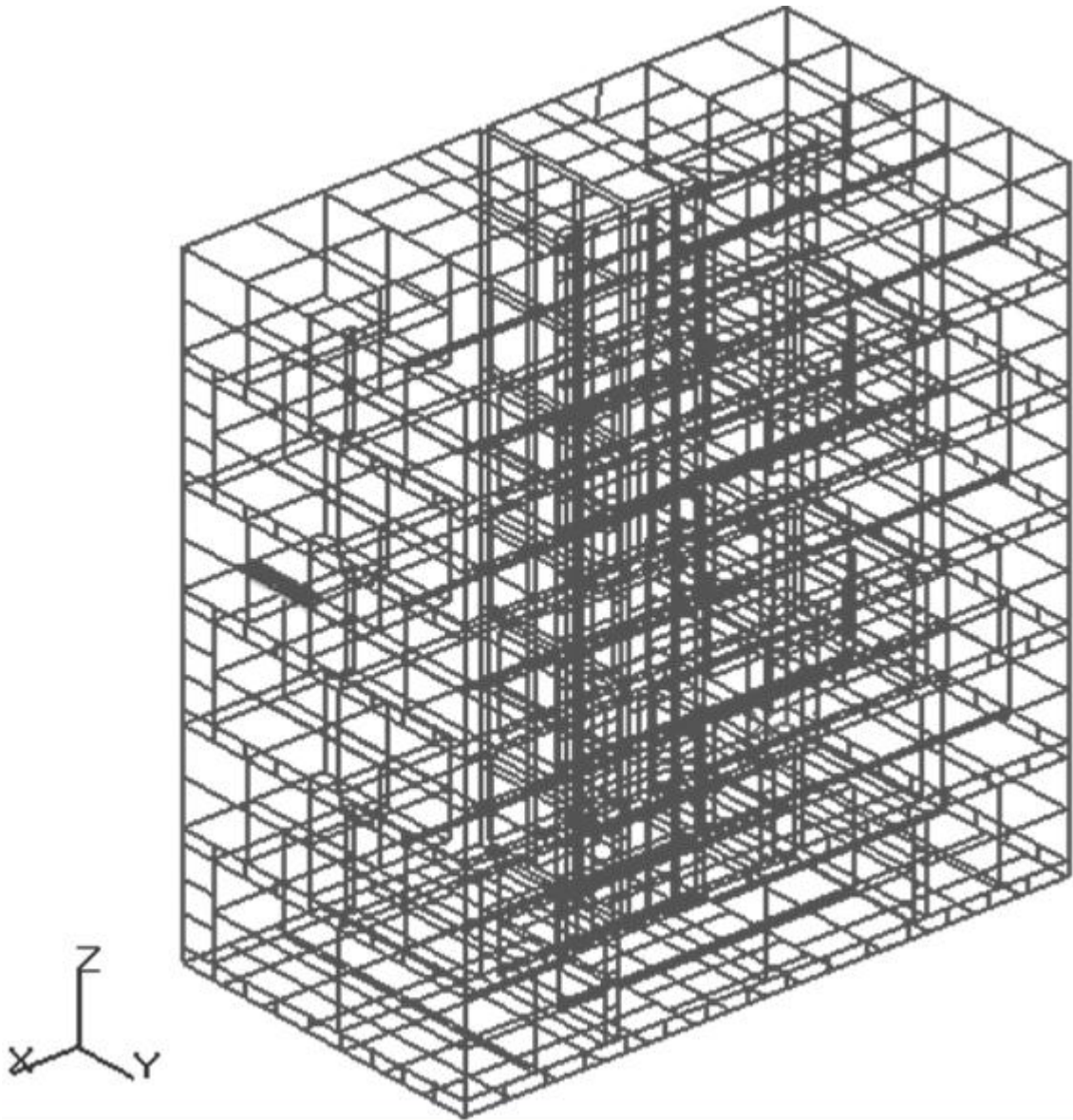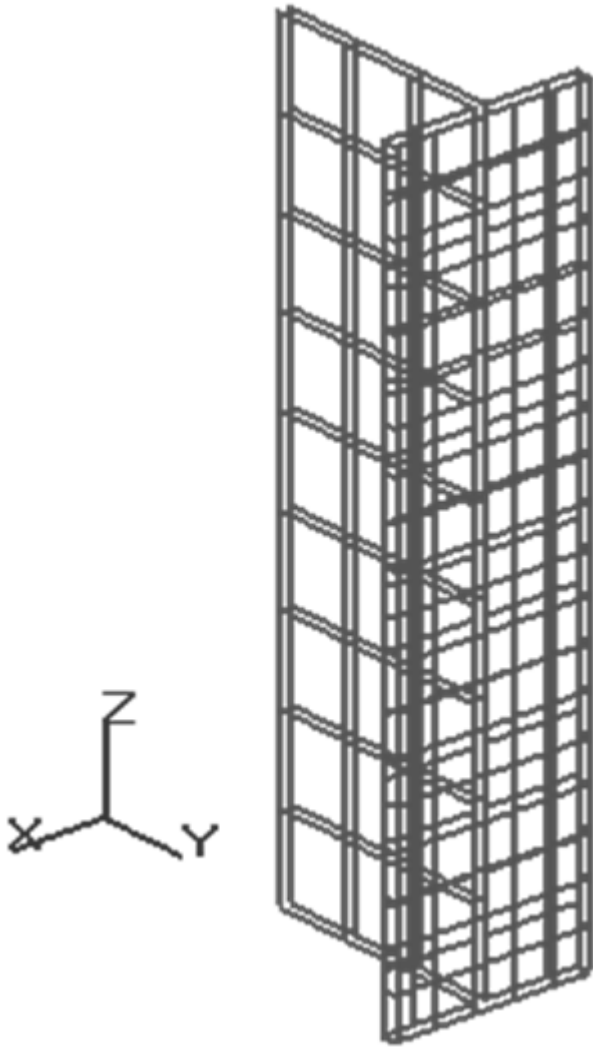
Figure 7: Potential distribution on the surface of mortar (mV vs CSE, symmetric in plane X=0, Case 1)
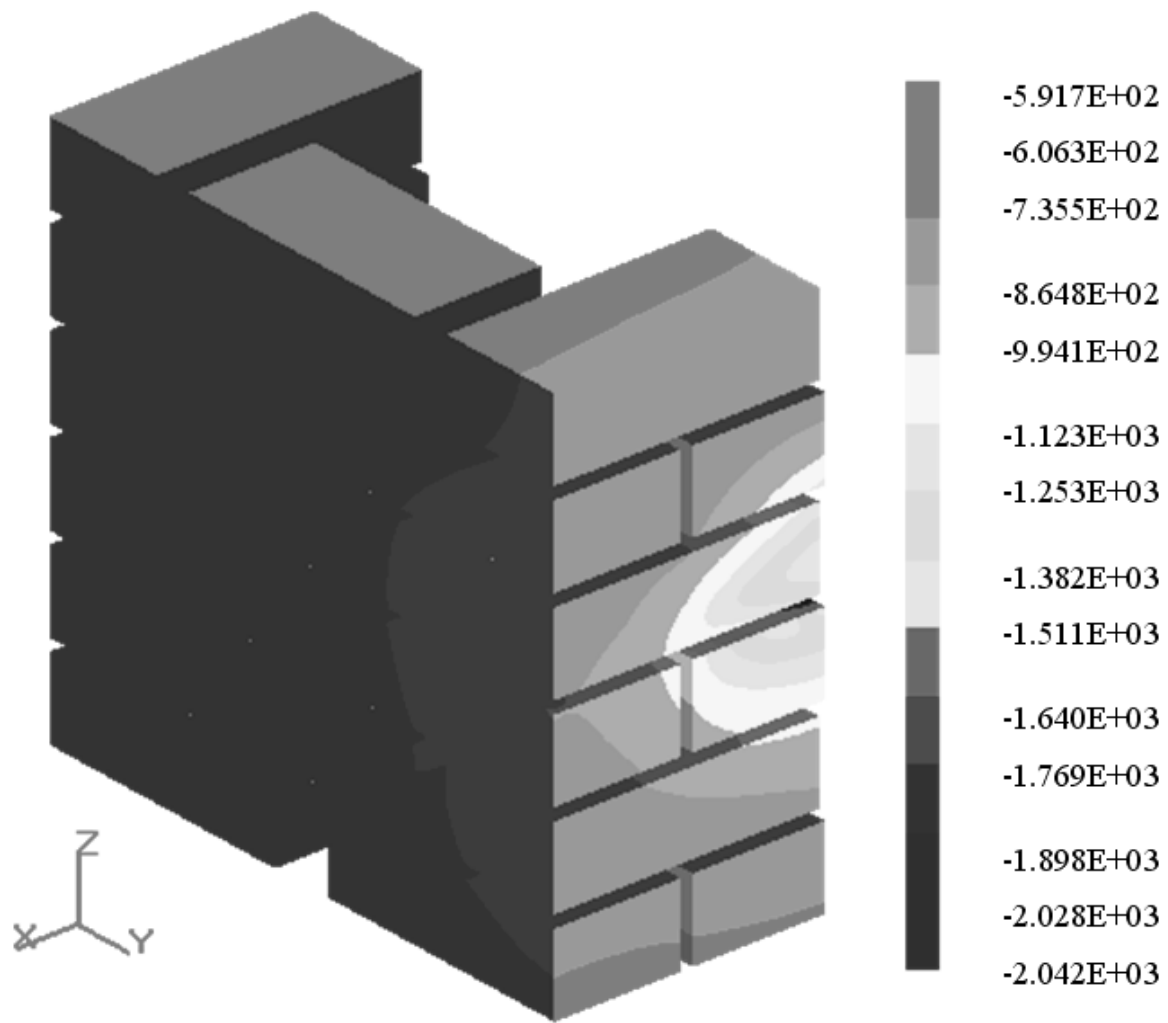
Figure 8: Potential distribution on the surface of brick (mV vs CSE, symmetric in plane X=0, Case 1)
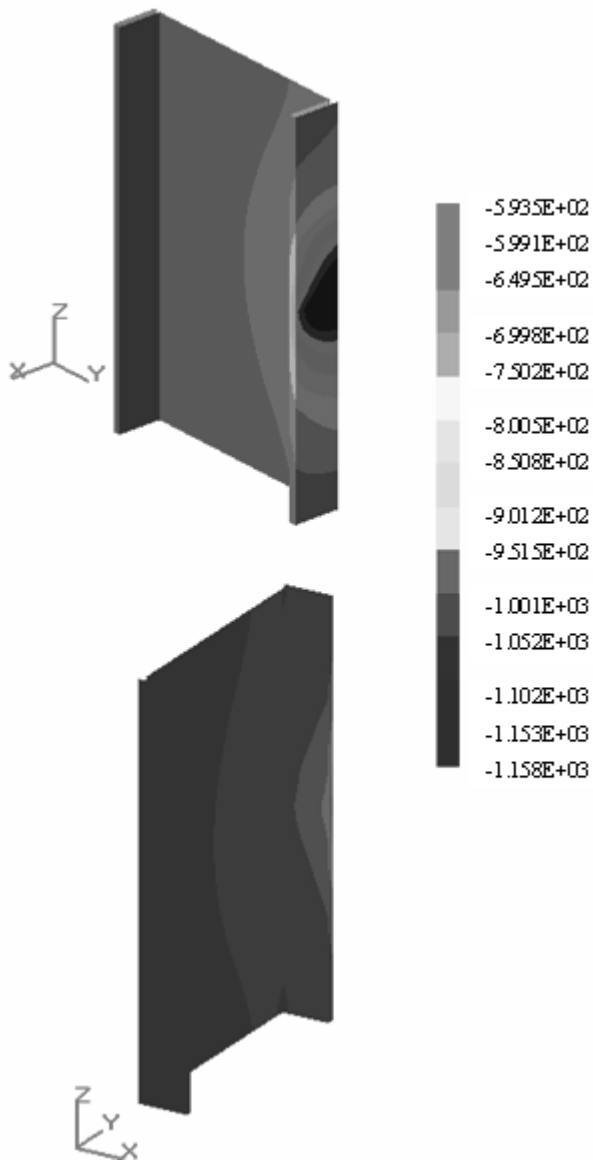
Figure 9: Potential distribution on the surface of steel (mV vs CSE, symmetric in plane X=0, Case 1)

Figure 10: Schematic representation of the total boundary element mesh on the surface of specimen (Symmetric in plane Y=0, Case 2)

Figure 11: Schematic representation of the boundary element mesh on the surface of steel piece (Case 2, symmetric in plane Y=0)
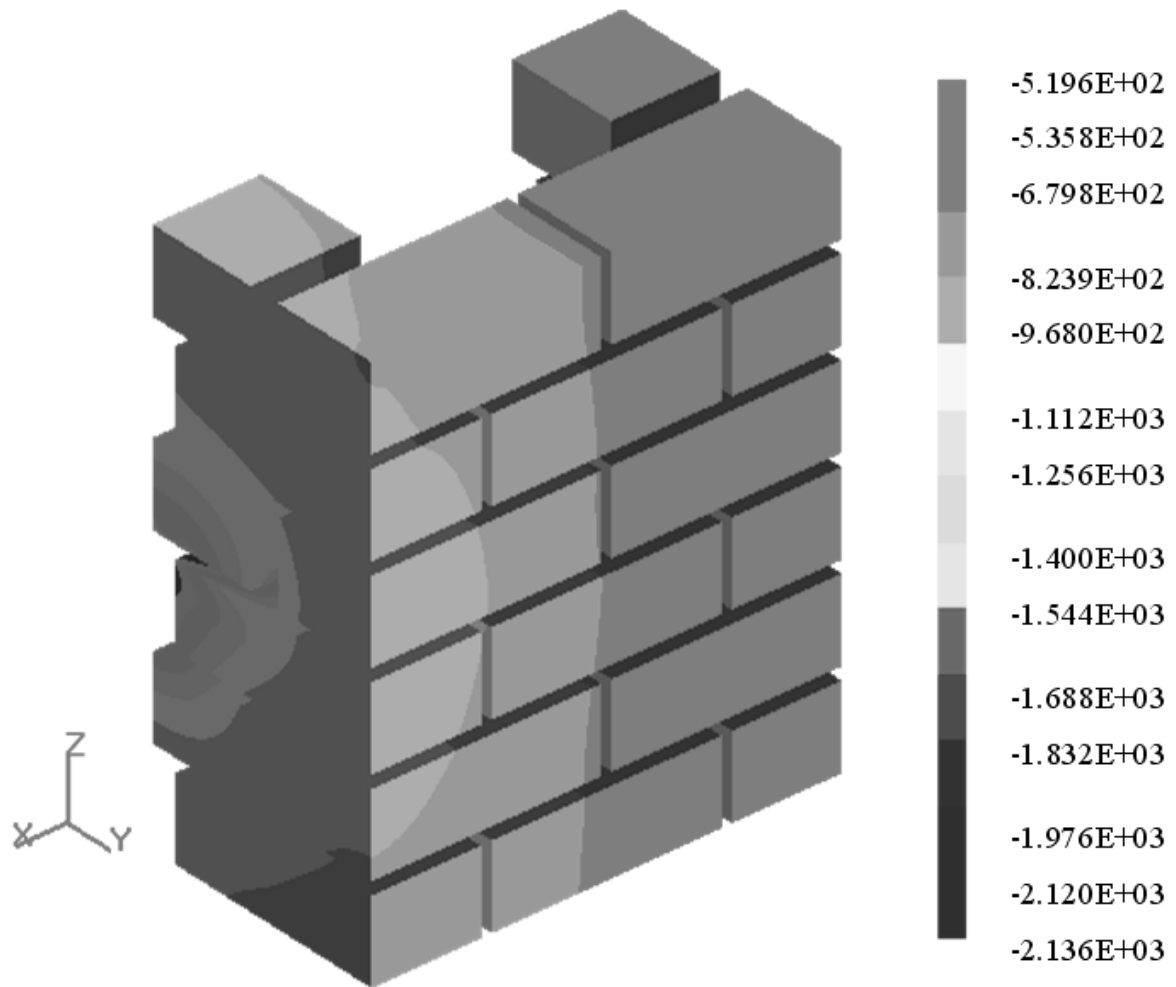
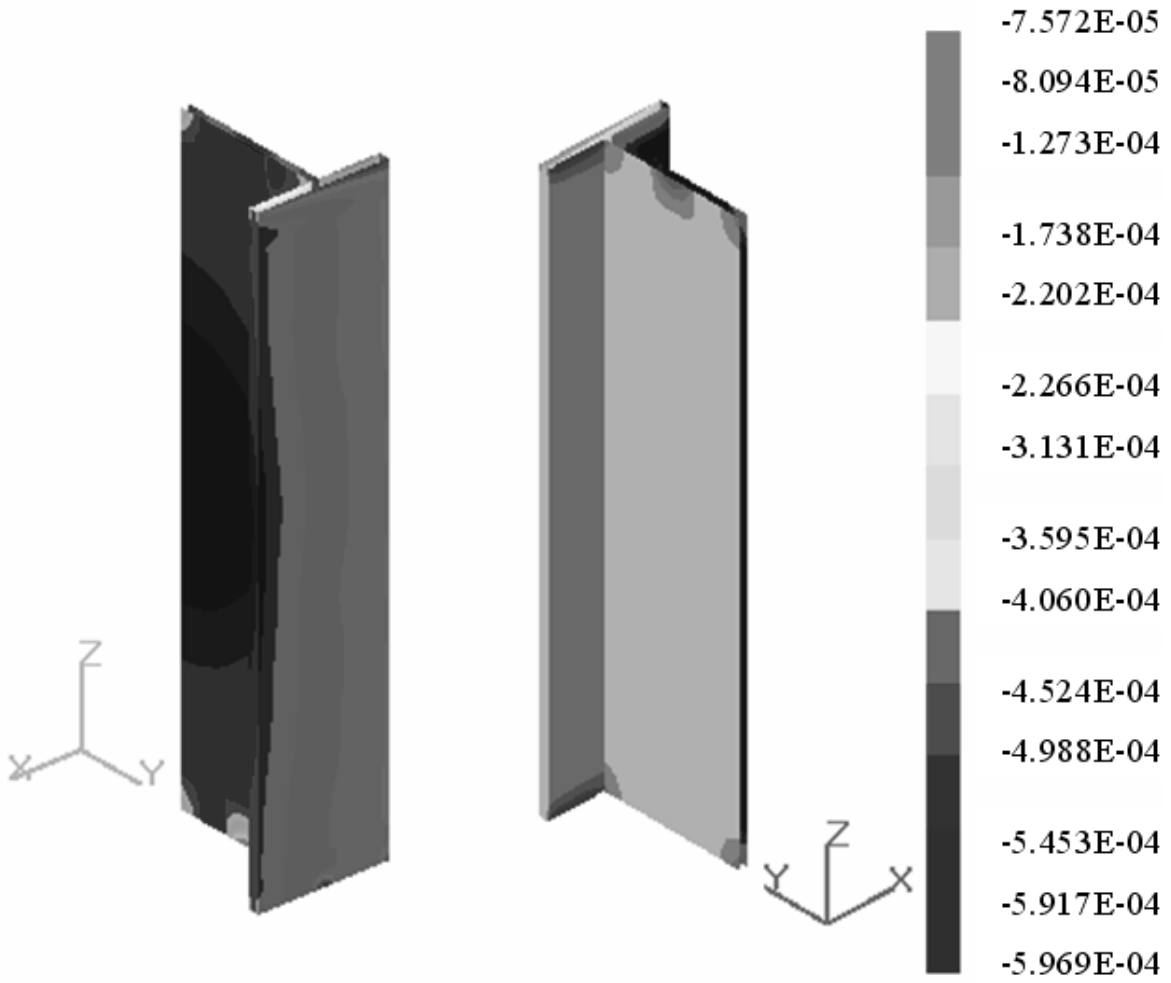Figure 12: Potential distribution on the surface of brick (mV vs CSE, symmetric in plane Y=0, Case 2)

Figure 13: Normal current distribution on the surface of steel (mA/cm^2, - current in, + current out, symmetric in plane Y=0, Case 2)
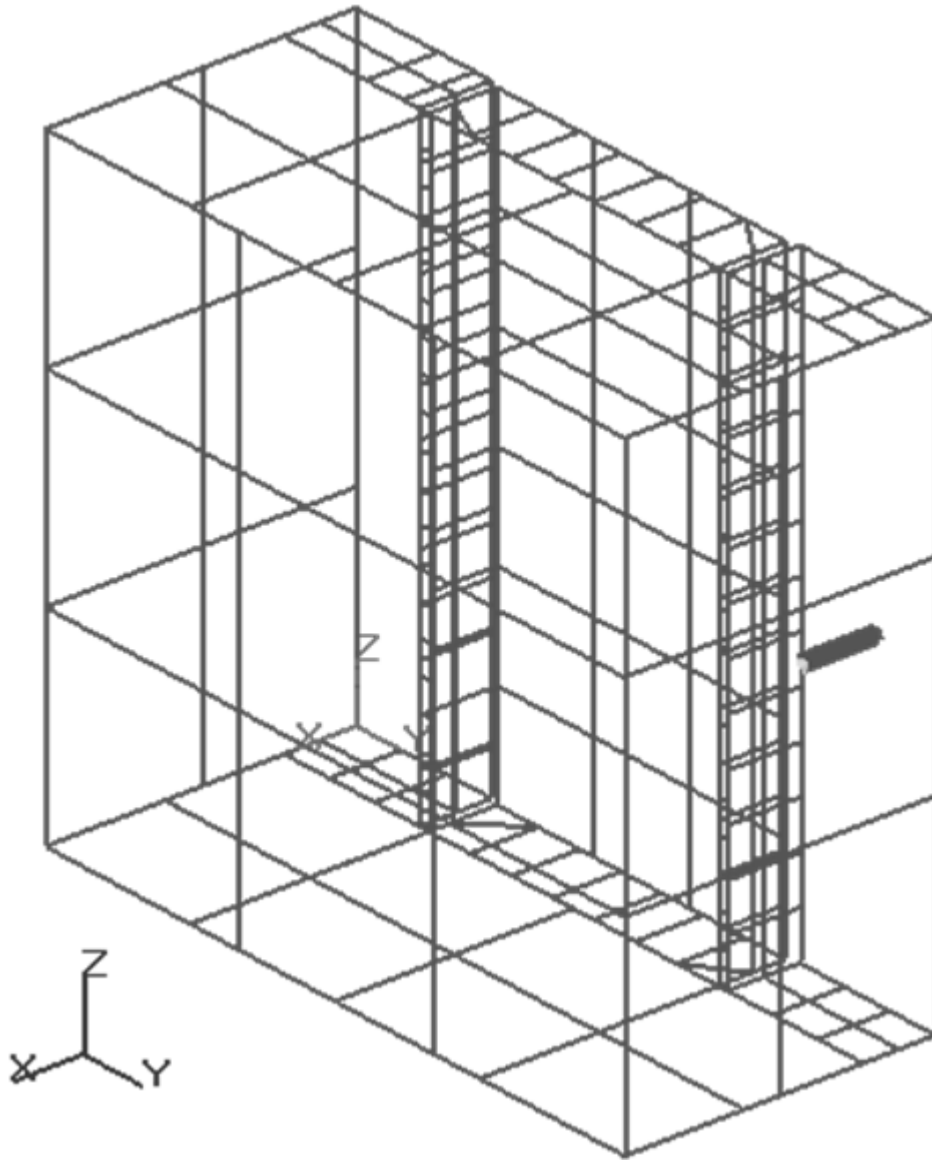
Figure 14: Schematic representation of the total boundary element mesh (Case 3, symmetric in plane X=0)
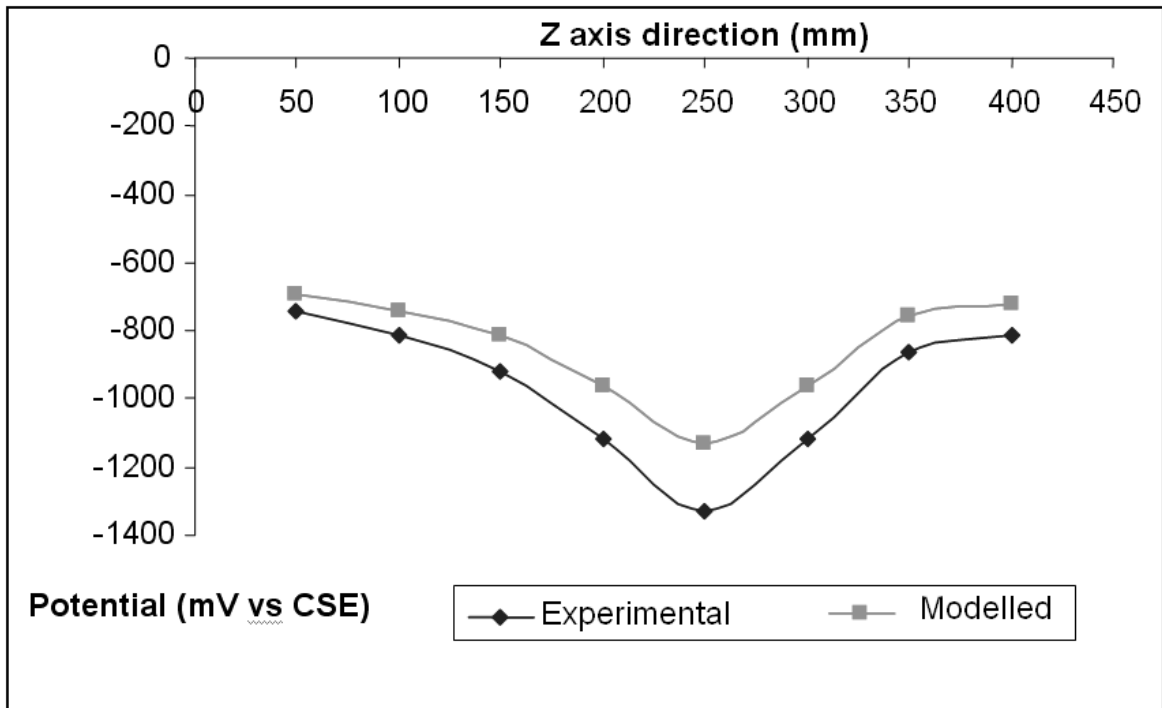
Figure 15: Comparison of experimental and modelled potential distribution (Case 1)